HHS Public Access

Author manuscript

Radiat Res. Author manuscript; available in PMC 2016 March 04.

Published in final edited form as:

Radiat Res. 2015 March ; 183(3): 291–304. doi:10.1667/RR13828.1.

Energy Metabolism in a Matched Model of Radiation Resistance for Head and Neck Squamous Cell Cancer

Jade Mims[a], **Nidhi Bansal**[a], **Manish S. Bharadwaj**[b], **Xiaofei Chen**[a], **Anthony J. Molina**[b], **Allen W. Tsang**[a], and **Cristina M. Furdui**[a,1]

[a]Section on Molecular Medicine, Department of Internal Medicine, Wake Forest School of Medicine, Winston-Salem, North Carolina 27157

[b]Section on Gerontology and Geriatric Medicine, Department of Internal Medicine, Wake Forest School of Medicine, Winston-Salem, North Carolina 27157

Abstract

While radiation therapy is commonly used for treating cancer, radiation resistance can limit long-term control of the disease. In this study, we investigated the reprogramming of the energy metabolism in radiosensitive and radioresistant head and neck squamous cell carcinomas (HNSCC) using a preclinical matched model of radiation resistance. Our investigation found that radioresistant rSCC-61 cells: 1. They display increased glucose uptake and decreased fatty acid uptake; 2. They deviate from the classical Warburg effect by diverting the glycolytic flux into the pentose phosphate pathway; 3. They are more dependent on glucose than glutamine metabolism to support growth; 4. They have decreased mitochondrial oxidative phosphorylation; 5. They have enhanced fatty acid biosynthesis by increasing the expression of fatty acid synthase; and 6. They utilize endogenous fatty acids to meet the energy demands for proliferation. Inhibition of fatty acid synthase with orlistat or FASN siRNA resulted in increased cytotoxicity and sensitivity to radiation in rSCC-61 cells. These results demonstrate the potential of combination therapy using radiation and orlistat or other inhibitors of lipid and energy metabolism for treating radiation resistance in HNSCC.

INTRODUCTION

Head and neck squamous cell carcinomas (HNSCC) accounts for nearly 3% of all new cancers in the U.S. and has an annual incidence of 500,000 new cases worldwide (1). The treatment options available for HNSCC patients utilize various combinations of surgery, radiation therapy and chemotherapy, depending on the stage and resectability of the disease. Radiation therapy alone or combined with chemotherapy can be a primary curative treatment prescribed for these patients either as definitive or as adjuvant post-surgical therapy. Significant acute and long-term side effects (e.g., oral mucositis, dysphagia) as well as the development of therapy resistant tumor cells can limit the effective use of radiation therapy. For these reasons, there is an increased focus on the use of targeted radiosensitizing

[1]Address for correspondence: Wake Forest School of Medicine, Internal Medicine, Medical Center Blvd., Winston-Salem, NC, 27157; cfurdui@wakehealth.edu.

agents used in combination with radiation therapy to treat radiation-resistant tumors, and potentially reduce normal tissue toxicity. Because of the increased expression of epidermal growth factor receptor (EGFR) found in >80% of HNSCC cases (2), this protein is considered as an attractive target for HNSCC treatment. In 2007, the FDA approved the first targeted therapy against EGFR (Cetuximab, a monoclonal antibody against EGFR), to be used in conjunction with radiation therapy in patients with locally advanced HNSCC based on the clinical studies reported by Bonner *et al*. (3). However, despite the wide overexpression of EGFR in HNSCC, only 10–15% of patients respond to this treatment, suggesting a need for additional targets (4).

The reprogramming of cancer cell metabolism has gained recent attention as one of the major hallmarks of cancer (5, 6). The rewiring of tumor cell metabolism is recognized as a dynamic process adopted by cancer cells to ensure a steady supply of metabolites for generation of both biomass and energy (7, 8). A seminal finding for this metabolic diversion is the Warburg effect (9), which allows for conversion of glucose into lactate instead of pyruvate even when sufficient oxygen is available to support mitochondrial oxidative phosphorylation (OXPHOS). The advantage of this process for energy production is the buildup of glycolytic intermediates, which can provide for the biosynthetic needs of daughter cells after cell division (10). The Warburg effect is often misinterpreted as an indicator of damaged mitochondrial function in tumor cells (11). However, more recent reports show that mitochondrial function in cancer cells is intact and although these cells may not maximize their ATP production through mitochondrial OXPHOS, a significant fraction of the ATP might still be derived from it (12). In addition, cancer cells are known to utilize mitochondrial enzymes to meet their challenge of macro-molecular biosynthesis and ensure effective cellular proliferation (12). Over the past years, a number of studies have addressed the diversity of tumor energy metabolism and identified the mechanistic connections between metabolism, signaling and cancer cell proliferation (13). It is now recognized that tumor cells demonstrate metabolic heterogeneity with capacity to utilize alternative oxidizable substrates such as glutamine and fatty acids (14–16). Therefore, interference with tumor cell metabolism is emerging as a novel treatment strategy in many types of malignancies including HNSCC (17–23).

Previous investigations of HNSCC metabolism have revealed dysregulation of multiple metabolic pathways such as OXPHOS, TCA cycle and glutaminolysis (19), as well as a general reliance on glucose as the dominant energy source for survival and proliferation (17). However, to our knowledge, the metabolic changes associated with radiation-resistant tumor cells in HNSCC have not been investigated. Thus, a better understanding of the underlying molecular and metabolic regulation that leads to radiation-resistant cells in HNSCC could significantly aid in the introduction of more effective and novel therapeutics. In an effort to underpin the molecular reprogramming associated with the acquisition of radiation resistance in HNSCC, we developed a matched model of radiation-resistant cells for this disease, the SCC-61/rSCC-61 system, which we reported on previously (24). Quantitative proteomic profiling showed broad changes in protein expression in the radioresistant cells (rSCC-61) that were associated with cellular metabolism, in addition to the expected upregulation of proteins involved in protection against DNA damage (24).

In this study, we followed up on the findings from the proteomics analysis and investigated the reprogramming of energy metabolism in the SCC-61/rSCC-61 matched model of radioresistant cells. We found that radioresistant rSCC-61 cells deviate from the classical Warburg effect by diverting the glycolytic flux into the pentose phosphate pathway (PPP). Additionally, these cells have decreased mitochondrial OXPHOS, and increased expression of fatty acid synthase (FASN), which is related to increased reliance on the utilization of endogenous fatty acids for energy production. Inhibition of FASN with orlistat or FASN siRNA resulted in increased cytotoxicity and sensitivity to radiation treatment in rSCC-61 cells. Bioenergy studies showed decreased ATP synthesis and lower spare respiratory capacity as potential mechanisms of increased sensitivity to radiation in orlistat-treated rSCC-61 cells.

MATERIALS AND METHODS

Reagents

Antibodies and reagents were obtained from the following sources: rabbit anti-COXIV, rabbit anti-glucose 6-phosphate dehydrogenase, rabbit anti-β actin and goat anti-rabbit IgG HRP (Cell Signaling Technology®, Danvers, MA); mouse anti-FASN (BD Biosciences, San Jose, CA); rabbit anti-GAPDH (Millipore, Billerica, MA); mouse anti-TIGAR and rabbit anti-mouse IgG HRP (Santa Cruz Biotechnology, Dallas, TX); Dulbecco's modified Eagle medium (DMEM)/F12 and fetal bovine serum (FBS) (Gibco/Invitrogen™, Carlsbad, CA); phosphate buffered saline (PBS) (Lonza Group Ltd., Basel, Switzerland); sulforhodamine B (SRB) for measuring cell proliferation (Sigma-Aldrich® LLC, St. Louis, MO); bicinchoninic acid (BCA) protein estimation kit and Western Lightning® Plus-ECL (Thermo Fisher Scientific Inc., Boston, MA). Orlistat was kindly provided by the laboratory of Prof. Steven Kridel, Department of Cancer Biology, Wake Forest University Health Sciences, Winston-Salem, NC. FASN siRNA was purchased from Dharmacon™ (Thermo Fisher Scientific Inc.), and ^{14}C-palmitate and 2-deoxy-D-[3H] glucose were purchased from PerkinElmer® Inc. (Waltham, MA).

Cell Culture and Radiation Treatment

The generation of the SCC-61/rSCC-61 matched model of response to radiation was described earlier (24). Briefly, the radiation-sensitive SCC-61 cells were irradiated *in vitro* with fractionated ionizing radiation (8 × 2 Gy), the resulting cell population was plated on soft agar and a single colony (rSCC-61) was picked for in-depth analysis of the mechanisms driving the response to radiation treatment in HNSCC. Both SCC-61 and rSCC-61 cells used in this study were cultured in the DMEM/F12 medium supplemented with 10% FBS (Invitrogen) at 37°C and 5% CO_2. Cell medium was replaced every two days with fresh medium. Where applicable, a 444 TBq 12,000 Ci self-shielded ^{137}Cs (Cesium) irradiator was used for radiation treatment. Culture dishes were placed on a Styrofoam insert within the chamber of the irradiator, such that the distance from the cesium source would result in a homogenous dose distribution over the desired field with a dose rate of 392 rad/min. From the dose rate, the exposure time required to deliver the desired dose was calculated and entered into the irradiator.

Glucose Uptake

SCC-61 and rSCC-61 cells were grown in six-well plates to 70% confluency. Medium was then removed and cells were washed two times with PBS at room temperature. The assay was initiated by the addition of 0.1 m*M* 2-deoxyglucose and 0.5 μCi/mL 2-deoxy-D-[3H] glucose (PerkinElmer) and terminated after 30 min by washing cells two times in ice-cold PBS and quenching with 0.05 *M* NaOH. Uptake of 2-deoxy-D-[3H] glucose was detected in ScintiVerse™ BD scintillation mixture (Thermo Fisher Scientific) using a Beckman LS 6000 SC scintillation counter and was normalized by protein concentration.

Cell Proliferation Using SRB Assay

The proliferation of SCC-61 and rSCC-61 cells in response to glucose or glutamine deprivation, 6-aminonicotinamide (6-AN) (Sigma-Aldrich® LLC, St. Louis, MO) or 2-deoxy-D-glucose (2-DG) (Sigma-Aldrich) or orlistat treatment was determined using the SRB colorimetric assay. The cells were seeded in 24-well plates at a density of 50,000/well in 1 mL. After overnight incubation at 37°C, the cells were either incubated in glucose-free or glutamine-free medium, or treated with either 5 μ*M* 6-AN, 20 m*M* 2-DG or 0.1–100 μ*M* orlistat and then given 0 Gy or 2 Gy irradiation and incubated for an additional 48 h at 37°C. For experiments involving glutamine deprivation the treated cells were incubated for 72 h at 37°C. After incubation, cells were fixed with 500 μL cold 10% trichloroacetic acid (TCA) and incubated at 4°C for 1 h. After fixing, cells were washed 4× with water and dried completely before the addition of 100 μL of 0.057 % (wt/vol) SRB solution to each well for 30 min at room temperature. Plates were quickly rinsed 4× with 1% (vol/vol) acetic acid to remove unbound dye and dried completely. Next, 200 μL of 10 m*M* Tris base solution (pH 10.5) was added to each well and then shaken for 30 min to solubilize protein-bound dye. The absorbance was measured at 510 nm using a microplate reader.

GLUT1 Imaging Analysis

SCC-61 and rSCC-61 cells were seeded in 1 mL Microtek chambers at a density of 2×10^4 cells/mL and incubated overnight at 37°C and 5% CO_2. After overnight incubation, cells were washed with cold PBS, fixed in 4% formaldehyde for 15 min and permeabilized with 0.1% Triton X-100 followed by blocking with 5% BSA for 1 h at room temperature. The cells were incubated with 1:200 dilution of rabbit anti-GLUT1 (Millipore) overnight at 4°C followed by washing 3× with PBS, incubation with 1:1,000 dilution of secondary anti-rabbit Alexa Fluor® 488 conjugate for 1 h at room temperature and 10 min incubation with 1:1,000 Hoescht before mounting with Fluoromount™ (Sigma-Aldrich). Imaging was performed using a Zeiss LSM710 confocal microscope and a 40× objective. LSM image browser was used for processing the confocal images.

Mitochondrial Stress Assays Using the Seahorse XFA 24-3 System

Measurement of OCR under normal growth conditions—O_2 consumption was determined using a Seahorse XFA 24-3 system. SCC-61 and rSCC-61 (4×10^4 cells) were seeded in the 24-well XF24 cell culture plate in DMEM/F12 (+10% FBS) and allowed to grow for 24 h. One hour prior to analysis, culture media was replaced by XF assay medium supplemented with glucose (17.5 m*M*) and sodium pyruvate (0.5 m*M*) and incubated at

37°C for 1 h to allow pH and temperature stabilization in a non-CO_2 incubator. The OCR was repeatedly measured for a total of 5 measurements followed by sequential injection of oligomycin (0.75 μ*M*), FCCP (1 μ*M*) and antimycin A/rotenone (1 μ*M* each), after measurements 5, 9 and 15, respectively. After all measurements were completed, cells were lysed and protein estimation was performed by BCA assay to confirm equal distribution of cells per well and to correct the OCR readings by protein concentration if needed. All data were analyzed using XF software and displayed as average OCR (p*M*/min). The data is the average of replicate wells (n = 3–5) ± SEM.

Fatty acid oxidation (FAO) assay using cells treated with exogenous palmitate—Similarly to above, 4×10^4 cells were seeded in the 24-well XF24 cell culture plate in DMEM/F12 (+10% FBS) and allowed to grow for 24 h. At 24 h prior to analysis, culture media was replaced by substrate limited media supplemented with glucose (0.5 m*M*), GlutaMAX (1 m*M*), carnitine (0.5 m*M*) and 1% FBS and incubated at 37°C to prime the cells to oxidize exogenous fatty acids. Culture media was replaced by FAO assay medium (111 m*M* NaCl, 4.7 m*M* KCl, 1.25 m*M* $CaCl_2$, 2 m*M* $MgSO_4$, 1.2 m*M* NaH_2PO_4) supplemented with 2.5 m*M* glucose, 0.5 m*M* carnitine and 5 m*M* HEPES, and preheated at 37°C for 1 h in a non-CO_2 incubator. A final concentration of 1.2 m*M* BSA or XF Palmitate-BSA substrate was added to the appropriate wells immediately before the start of assay. The OCR was measured repeatedly 4 times and after the sequential injection of oligomycin (0.75 μ*M*), FCCP (1 μ*M*) and antimycin A/rotenone (1 μ*M* each), added after measurements 4, 7, and 10, respectively. After all measurements were completed, cells were lysed, protein concentration was measured by the BCA assay and data was processed as described above.

Measuring orlistat effects on OCR—The same procedure was followed as described for the assays under normal growth conditions with the only difference being pretreatment of cells with 10 μ*M* orlistat for 2.5 h before the start of the experiment. After all measurements were completed, cells were lysed, protein concentration was measured by the BCA assay and data was processed as described above.

Detection of mitochondrial reactive oxygen species—Subconfluent SCC-61 and rSCC-61 cells were treated with 20 m*M* 2-DG for 24 h, stained with 0.5 μ*M* MitoSOX™ Red (Ex/Em 500/580, designated red) and imaged. Imaging was performed using a Zeiss LSM 710 confocal microscope and a 10× objective. All images were collected under the same confocal settings. LSM image browser was used for processing the confocal images.

NADPH/$NADP^+$ Quantification

Cells were seeded at 1×10^5, allowed to attach, and then washed with cold PBS immediately after attachment. Cells were extracted with 200 μL of $NADP^+$/NADPH extraction buffer by homogenization, then vortexed for 10 s, followed by centrifugation at 13,000*g* for 10 min to remove insoluble material. Samples were deproteinized before use in assay by filtering through a 10 kDa cutoff spin filter. To detect NADPH, $NADP^+$ was decomposed by centrifuging tubes and heating to 60°C for 30 min in a water bath followed by cooling on ice. Samples were quickly spun to remove any precipitates, leaving only NADPH. $NADP^+$

and NADPH samples were incubated with Master Reaction mixture for 2 h before absorbance was measured at 450 nm according to the manufacturer's (cat. no. MAK038; Sigma-Aldrich) protocol.

Clonogenic Cell Survival Assay

Radiation-resistant rSCC-61 cells and the parental SCC-61 cells were trypsinized, resuspended in complete medium (DMEM/F12 + 10% FBS) and plated (250 cells/well) into the 6-well culture dishes. After overnight incubation at 37°C, the cells were treated with a range of concentrations of orlistat in triplicates (0.5–100 μ*M*) and allowed to incubate for 16 h. Fresh media was then added and the cells were incubated for additional 7–8 days for the colony formation. Once formed, the colonies were fixed in methanol and acetic acid (1:1) solution and stained with 0.5% crystal violet. The colonies containing more than 50 cells were scored as clonogenic survivors. The surviving fraction of the drug-treated cells was normalized using the plating efficiencies of their corresponding untreated control.

Fatty Acid Synthase Activity (FASN) Assay

Cells were harvested by treatment with trypsin-EDTA solution, pelleted by centrifugation, washed twice, and resuspended in cold PBS. Cells were sonicated for 30 min at 4°C and centrifuged for 15 min at 4°C to obtain particle-free supernatants. A supernatant sample was taken to measure protein content by BCA assay. One μg/μL of total protein was used for the assay and 120 μL of this particle-free supernatant were pre-incubated for 15 min at 37°C for temperature equilibration. The sample was then added to 150 μL of the reaction buffer [200 m*M* potassium phosphate buffer (pH 7.0), 1 m*M* EDTA, 1 m*M* DTT, 30 μ*M* acetyl-CoA, 0.24 m*M* NADPH], followed by 30 μL of 500 μ*M* malonyl-CoA (FASN substrate), and the final volume of 0.3 mL of reaction mixture was assayed for 20 min to determine FASN-dependent oxidation of NADPH. Before the addition of malonyl-CoA, the background rate of NADPH oxidation in the presence of acetyl-CoA was monitored at 340 nm for 10 min.

siRNA Transfections and Clonogenic Assays

Cells were grown to 60% confluency followed by transfection with FASN siRNA (60 and 100 n*M*) or control siRNA (100 n*M*) (Dharmacon) according to manufacturer's protocol. After 36 h, transfected cells were trypsinized and resuspended in the complete medium and plated (500 cells/well) into the six-well culture dishes. After 4 h, the cells were irradiated with 2 Gy and incubated for an additional 7–8 days for the colony formation. Once formed, the colonies were fixed in methanol and acetic acid (1:1) solution and stained with 0.5% crystal violet. The colonies containing more than 50 cells were scored as clonogenic survivors. The surviving fraction of the irradiated cells was normalized using the plating efficiencies of their corresponding untreated control. SCC-61 cells were also included in the clonogenic assays. Western blot analysis was performed to confirm the depletion of FASN upon treatment of rSCC-61 cells with respective siRNAs.

^{14}C-Palmitate Uptake Assay

SCC-61 and rSCC-61 cells (2×10^5 cells) were seeded per well in a six-well plate and grown overnight at 37°C and 5% CO_2. On the following day, cells were washed, then

starved in HBSS for 30 min and subsequently washed twice with HBSS. The cells were then incubated with ^{14}C-labeled palmitate (1 μCi) for 30 min followed by three washes with PBS. The cells were collected in 0.5 *N* NaOH (500 μL) and transferred to scintillation vials containing 1 mL of scintillation fluid. The ^{14}C-palmitate uptake was expressed as n*M*/mg of total protein.

Western Blot Analysis

SCC-61 or rSCC-61 cells (8×10^5 cells) were seeded in 100 mm culture dishes. Cells were lysed after 48 h and the fresh media was replenished 24 h before lysis. Cells were lysed using RIPA buffer [20 m*M* Tris-Cl (pH 7.4); 150 m*M* NaCl (1% sodium deoxycholate); 1% Triton X-100 (0.1% SDS); supplemented with protease and phosphatase inhibitor tablets (Roche Diagnostics, Indianapolis, IN)]. The lysates were incubated on ice for 1 h followed by centrifugation at 10,000*g* for 10 min. The lysates were then normalized for their protein concentration across different treatment conditions and subjected to SDS-PAGE. The separated proteins were then transferred to a nitrocellulose membrane (0.45 μm; Bio-Rad Laboratories Inc., Hercules, CA) and probed for the indicated proteins using the corresponding primary and HRP-linked secondary antibodies. Proteins were visualized by treating the blots with the Western Lightning Plus-ECL reagents followed by exposure to autoradiography film (GeneMate Blue Ultra Autorad film; BioExpress, Kaysville, UT). Quantification of Western blot results was performed using ImageJ (National Institutes of Health, Bethesda, MD).

Statistical Analysis

Statistical analysis (*t* test) was based on a minimum of three biological replicates using SigmaPlot™ (Systat® Software Inc., San Jose, CA), version 12.0 or Microsoft Excel 2010. Asterisks indicate statistically significant changes compared with untreated controls (α = 0.05, **P* = 0.01–0.05, ***P* = 0.001–0.01 and ****P* = <0.001).

RESULTS

Contribution of Glycolysis to SCC-61 and rSCC-61 Proliferation

We examined the glucose uptake and utilization in radiosensitive SCC-61 and radioresistant rSCC-61 cells. The total glucose uptake of rSCC-61 cells was significantly higher than the SCC-61 cells ($P < 0.001$; Fig. 1A), consistent with the increased expression and membrane localization of glucose transporter GLUT1 in rSCC-61 determined by imaging and Western blot ($P < 0.001$; Fig. 1B). To further determine the requirement for glucose metabolism in rSCC-61 cells, we examined cell viability under glucose deprivation with 0 and 2 Gy irradiation. Cells were grown using regular media, media depleted of glucose or regular media supplemented with 2-DG, a glycolysis inhibitor, followed by radiation treatment. Cell proliferation was measured using the SRB assay (25). Regardless of radiation treatment, both glucose starvation and 2-DG treatment significantly reduced cell proliferation in both rSCC-61 and SCC-61 cells, although the effect was more pronounced in rSCC-61 (e.g., ~twofold vs. ~fourfold decrease in cell proliferation in glucose-deprived SCC-61 and rSCC-61 cells, respectively, in the absence of radiation treatment; $P < 0.001$; Fig. 1C).

Contribution of PPP to SCC-61 and rSCC-61 Proliferation

Multiple levels of regulation on glycolysis have been identified that can divert glucose towards the synthesis of molecular building blocks that are fundamental to cancer cell proliferation. For example, TP53-inducible glycolysis and apoptosis regulator (TIGAR) has fructose-2,6-bis-phophatase activity and is an established regulator of glycolysis and PPP (26). Increased expression of TIGAR inhibits glycolysis and promotes PPP by lowering fructose-2,6-bisphosphate and increasing fructose-6-phosphate in cells. One of the mechanisms underlying glycolysis/PPP regulation is the conversion of fructose-6-phosphate into glucose-6-phosphate, the substrate for the rate-limiting reaction in the PPP catalyzed by glucose-6-phosphate dehydrogenase (G6PD). The parallel decrease in fructose-2,6-biphosphate results in downregulation of phosphofructokinase 1 activity, a glycolytic enzyme catalyzing the conversion of fructose-6-phosphate to form fructose-1,6-bisphosphate. Western blot analysis showed increased expression of TIGAR ($P = 0.004$) and G6PD ($P < 0.001$) in rSCC-61, suggesting an increased routing of glucose into the PPP (Fig. 2A). In addition, quantitative proteomics analysis reported earlier showed a 3.5-fold increased expression in rSCC-61 of the enzyme 6-phosphogluconate dehydrogenase (6PGD) catalyzing the second NADPH producing step in the oxidative phase of PPP (24). Based on these results, we hypothesized that rSCC-61 would be more dependent on PPP than SCC-61. Indeed, treatment of SCC-61 and rSCC-61 cells with the 6-phosphogluconate dehydrogenase inhibitor, 6-aminonicotinamide, resulted in decreased cell proliferation in rSCC-61 compared with SCC-61 in both irradiated and control cells ($P = 0.005$ and $P = 0.008$, respectively; Fig. 2B). The expected consequence of upregulated PPP is increased production of NADPH and ribose-5-phosphate for subsequent biosynthesis of nucleic acids and defense against radiation-induced oxidative damage (27). Indeed, quantification of $NADPH/NADP^+$ ratio showed NADPH to be increased 1.5-fold in rSCC-61 compared to SCC-61 cells ($P = 0.04$; Fig. 2C). These results are also consistent with the functional analysis of our previously published quantitative proteomic data for SCC-61 and rSCC-61 cells, which showed significantly increased nucleotide metabolism, DNA replication and base excision repair in rSCC-61 (24).

Glutamine Utilization in SCC-61 and rSCC-61 Cells

Metabolic rewiring to satisfy rapid proliferation often includes utilization of secondary nutrient glutamine as a source for energy and biomass generation (8, 28, 29). Previously published data from a panel of 15 HNSCC cell lines indicated that glucose, not glutamine, is the dominant energy source for proliferation and survival of HNSCC cells (17). To demonstrate the preference of glucose and glutamine utilization in radiosensitive and radioresistant HNSCC, we investigated the effect of glutamine depletion without and with radiation treatment on rSCC-61 and SCC-61 proliferation. SCC-61 and rSCC-61 cells were cultured in the medium containing various concentrations of glutamine (0–2.5 m*M*) and cell proliferation was determined using the SRB assay. As shown in Fig. 3, glutamine starvation resulted in significantly decreased proliferation of SCC-61 cells compared with rSCC-61 (e.g., $P < 0.001$ for 0 m*M* glutamine) indicating that the radioresistant rSCC-61 cells are largely dependent on glucose for meeting their energy and growth requirements and less dependent on glutamine compared with the SCC-61 cells. Interestingly, the effects of

glutamine depletion on cell proliferation seem to be much stronger than those induced by irradiation, as indicated by lack of a significant difference in cell proliferation between irradiated and control cells in the absence of glutamine as substrate. This result is consistent with the data presented in Figs. 1C and 2B, which suggested a dependence of radiation-induced cell death on cellular energy metabolism.

rSCC-61 Cells Have Reduced Mitochondrial OXPHOS

The results presented in Figs. 1 and 2 demonstrate an increased dependence on overall glucose metabolism in rSCC-61 cells and increased flux through PPP in these cells. We have reported previously that rSCC-61 cells have increased expression of lactate dehydrogenase B enzyme (favoring conversion of lactate to pyruvate) and decreased expression of lactate dehydrogenase A (favoring conversion of pyruvate to lactate) (24), which also pointed to a possible diversion from the conventional Warburg metabolism. Taken together, the data indicated that a significant proportion of glycolytic flux was diverted into lactic acid synthesis in SCC-61 while in rSCC-61 the upstream glycolytic intermediates were funneled into the PPP but also possibly into the TCA and mitochondrial electron transfer chain (ETC) to support OXPHOS. To investigate the relative proportion of glycolytic flux entering the TCA cycle and mitochondrial ETC in SCC-61 and rSCC-61 cells, we measured the oxygen consumption rate (OCR) at basal and in response to modulators of ETC function using the Seahorse XF24 extracellular flux analyzer. Inhibition of ATP synthase with oligomycin was used to determine the proportion of OCR utilized for ATP production at basal conditions. Trifluorocarbonylcyanide phenylhydrazone (FCCP) was added to assess maximal uncoupled respiration and finally, rotenone/antimycin A was used to assess any residual nonmitochondrial OCR (Fig. 4A). Western blot analysis of the mitochondrial enzyme COXIV showed comparable mitochondrial content in SCC-61 and rSCC-61 cells (Fig. 4A). Six primary parameters were extracted using this methodology: basal respiration, ATP production, maximal respiration, spare respiratory capacity, proton leak and nonmitochondrial respiration (***$P < 0.001$, **$P < 0.01$; Fig. 4B). These parameters were calculated as shown by the highlighted areas under the SCC-61 data shown in Fig. 4A. There was a slight decrease in the proton leak in rSCC-61, however, this was not statistically significant. On the other hand, basal respiration, ATP production, maximal respiration, spare respiratory capacity, as well as the nonmitochondrial respiration were all statistically higher in SCC-61. Thus, we conclude that compared to SCC-61, the radiation-resistant rSCC-61 cells have decreased overall OXPHOS activity and ATP generation. These experiments also allow for detection and quantification of proton production or extracellular acidification rate (ECAR). The results show higher rates of proton production in SCC-61 cells compared with rSCC-61 cells (Fig. 4C). Overall, the results are consistent with the increased channeling of glycolysis intermediates into the PPP in rSCC-61 shown in Fig. 2, and with the increased proton secretion in SCC-61 (24). Thus, although there is more glucose uptake in rSCC-61 a greater proportion of this is funneled through the PPP and less through the mitochondrial ETC.

We then investigated whether the higher ROS content in SCC-61 compared with rSCC-61 reported earlier (24) could also be partly explained by the increased routing of glucose into the TCA and mitochondrial ETC in SCC-61 identified here. We used MitoSOX to determine

differences in mitochondrial ROS between the two cell lines and the consequence of 2-DG treatment on mitochondrial ROS generation. The results showed higher mitochondrial ROS in SCC-61 compared with rSCC-61 and decreased ROS with 2-DG treatment in SCC-61 consistent with the mitochondrial energy findings presented above. These results also show that the increased cytotoxicity of 2-DG in rSCC-61 is not due to an increase in mitochondrial ROS but more likely to decreased flux through PPP or possibly through other mechanisms, since 2-DG effects on cells extend well beyond blockage of glycolysis and PPP (30).

Contribution of Fatty Acid Metabolism to Energy Balance and Radiation Resistance in rSCC-61

Lipid metabolism is a major contributor to energy balance in cells, and while it is known to be upregulated in cancers (31), it has been less studied in relationship to radiation resistance. Since our previous quantitative proteomics studies identified a sevenfold increase in the expression of FASN in rSCC-61 relative to SCC-61 cells, we wanted to investigate the functional contribution of fatty acid metabolism (uptake, biosynthesis and oxidation) to energy balance and radiation response in these cells.

Fatty acid synthase (FASN) activity and uptake of exogenous fatty acids— First, we followed up on the proteomics findings with Western blot analysis showing a threefold increased expression of FASN ($P < 0.001$; Fig. 5A). The inconsistency in fold-change values is due to the limited linear dynamic range enabled by Western blot detection compared with the mass spectrometry-based quantitative analysis. Nevertheless, both analyses show a significant >3-fold increase of FASN in rSCC-61 cells. Next, we measured the FASN activity and detected a fivefold increased activity in rSCC-61 relative to SCC-61 ($P < 0.01$, Fig. 5B), which was consistent with the increased expression of FASN in these cells. We then hypothesized that the increased biosynthesis of fatty acids in rSCC-61 is associated with a decreased dependence on exogenous fatty acids. To address this, we quantified the uptake of fatty acids in SCC-61 and rSCC-61 cells using ^{14}C-palmitate and found a significant twofold decrease in both the amount and rate of palmitic acid uptake in rSCC-61 (Fig. 5C).

Fatty acid oxidation (FAO) assay shows decreased utilization of exogenous fatty acids to support mitochondrial OXPHOS in rSCC-61—SCC-61 and rSCC-61 FAO was determined using BSA conjugated palmitate as exogenous substrate. As shown in the OCR profile plots (Fig. 5D), the basal respiration in the presence of BSA:palmitate (purple box) was significantly higher than the BSA control (310 pM/min) in SCC-61 cells. The basal respiration under palmitate and BSA control treatment was calculated by subtracting the nonmitochondrial respiration (average of last three readings in each plot) from the average of the first four readings. The addition of BSA:palmitate to the rSCC-61 cells also resulted in an increase in basal respiration (85 pM/min) but this was lower than in SCC-61. The expected uncoupling of mitochondria by palmitate (blue box) was observed in both cell lines contributing to the basal respiration with 298 pM/min in SCC-61 and 228 pM/min in rSCC-61. The uncoupling of mitochondria by palmitate or BSA was calculated as the difference between the average of readings 5, 6 and 7 and the average of readings 11,

12 and 13 (nonmitochondrial respiration). Maximal respiration (green box) of SCC-61 due to utilization of exogenous palmitate was increased by 195 pM/min compared to 75 pM/min in rSCC-61. Maximal respiration was calculated as the difference between the average of readings 8, 9 and 10 and the average of readings 11, 12 and 13 (nonmitochondrial respiration). The results demonstrate significant reliance on utilization of endogenous fatty acids in radioresistant rSCC-61. While we do not currently understand the shift in basal OCR in rSCC-61 treated with BSA alone (control experiment), the significantly increased basal OCR in SCC-61 compared with rSCC-61 cells after the addition of palmitate correlates with the higher palmitate uptake seen in Fig. 5C.

Inhibition of FASN decreases rSCC-61 survival—Since tumor cells utilize fatty acids for multiple purposes (e.g., membrane synthesis, signaling, antioxidants) and the data in the FAO assay pointed to the need for endogenous fatty acid synthesis to support mitochondrial OXPHOS in rSCC-61, we next investigated the requirement for FASN activity in radiation resistance in rSCC-61. The rSCC-61 and SCC-61 cells were treated with orlistat, a pharmacological inhibitor of FASN, and cell survival was monitored using both clonogenic and cell proliferation assays. The results showed that compared to SCC-61 cells, rSCC-61 had decreased survival upon treatment with orlistat [rSCC-61 IC50 16.5 μ*M*, SCC-61 IC50 > 100 μ*M* (Fig. 6A)] and increased sensitivity to radiation [$P = 0.009$, $P = 0.005$, $P = 0.007$ for orlistat concentrations 0.1, 1.0 and 10.0 μ*M*, respectively (Fig. 6B)]. Next, we decreased the expression of FASN in rSCC-61 using a siRNA approach and quantified the consequence on the response to radiation. Overall, down-regulation of FASN with orlistat or siRNA treatment resulted in increased sensitivity to radiation in rSCC-61 cells ($P = 0.001–0.05$, Fig. 6C, left side) matching the response to radiation in SCC-61 cells, which were used as control in this experiment. The depletion of FASN protein upon transfection with FASN siRNA was confirmed by Western blot analysis (Fig, 6C, right side). To determine the role of endogenous fatty acids in mitochondrial OXPHOS activity in rSCC-61 cells, we inhibited FASN using 10 μ*M* orlistat and measured OCR as shown in Fig. 4B. The results showed inhibition of FASN by orlistat significantly decreased five out of six parameters extracted from the OCR data in rSCC-61 cells. In SCC-61, the orlistat treatment decreased only nonmitochondrial respiration while not affecting or slightly increasing some of the other OCR parameters (Fig. 6D). This data further supports the necessary role of fatty acid synthesis in OXPHOS activity and ATP generation in the radiation-resistant rSCC-61 cells and a potential contribution of fatty acid metabolism to nonmitochondrial respiration in both SCC-61 and rSCC-61 cells.

DISCUSSION

Despite significant advances in the understanding of HNSCC tumor biology, the management of HNSCC remains complicated and a multimodality approach is often employed to treat HNSCC patients. Radiation therapy is a common treatment for HNSCC and used in nearly all disease stages in combination with surgery or chemotherapy (32). However, despite recent progress on the use of targeted therapies (e.g., Cetuximab targeting epidermal growth factor receptor) in combination with radiation therapy to treat HNSCC, resistance to radiation treatment remains a serious concern (33–35). Ongoing efforts to

sensitize tumors to radiation treatment include improvements in radiation regimens and delivery, identification of molecular markers of radiation response, discovery of new therapeutic targets as sensitizers of radiation response and their optimization with existing radiation treatment options. Towards this goal, we had previously established a preclinical matched model of radiation resistance in HNSCC and performed comprehensive proteomics analysis to identify molecular networks that can contribute to the radiation-resistant phenotype in HNSCC (24). The study has now been extended to understand the nutrient and energy signatures of SCC-61 and the matched radiation-resistant rSCC-61.

Normal untransformed eukaryotic cells have evolved for optimal utilization of biochemical pathways (e.g., glycolysis, TCA, mitochondrial OXPHOS, PPP) to convert glucose into CO_2 and H_2O while maximizing the production of ATP, NADPH and various biosynthetic intermediates. In contrast, tumor cells have been traditionally classified as ‘‘addicted to glucose’’ where they employ aerobic glycolysis for energy generation and divert mitochondrial activity into biosyn-thetic pathways for biomass generation to support cell proliferation (12). In addition, studies have increasingly shown that tumor cells demonstrate utilization of alternative oxidizable substrates like glutamine and fatty acids to potentiate their survival (14–16). Despite the increased recognition of the need to understand tumor metabolism for improved disease management, few studies have focused on presenting a clear picture of the metabolic phenotype of HNSCC (17, 19, 36). Two earlier published studies showed NMR-based metabolic profiling of HNSCC tumor specimens and varied levels of metabolites that revealed dysregulation in multiple metabolic events, including the Warburg effect, TCA, glutaminolysis and antioxidant mechanisms, among others (19, 36). In another study by Sandulache *et al*. (17), a panel of 15 HNSCC cell lines was evaluated for metabolic phenotype and the potential for targeting key energy metabolism pathways for inhibiting cell proliferation in head and neck cancer. The majority of cell lines tested in this study relied on glucose and not glutamine for their survival. However, there remains a lack of coherent understanding of the metabolic perturbations that exist in the development of radioresistance in HNSCC. In the current study we show that radiation resistance is associated with increased glucose uptake consistent with the increased reliance of these cells on glycolysis and PPP. We identified increased expression of GLUT1, a clinically useful marker for HNSCC disease (37) and increased localization to the membrane in rSCC-61 cells compared to SCC-61 cells. While both SCC-61 and rSCC-61 cells were sensitive to metabolic inhibitors of glycolysis (2-DG) and PPP (6-AN), the effects of 2-DG and 6-AN in rSCC-61 were stronger than in SCC-61. Further analyses support the increased routing of glucose into the PPP pathway due to increased expression of TIGAR, G6PD and increased production of NADPH in rSCC-61 for synthesis of lipids and nucleic acids. These observations are in accordance with previous reports showing combinatorial treatment with 2-DG and 6-AN to radiosensitize head and neck cancer cells through mechanisms that involved redox-mediated alteration of ASK1-JNK/p38MAPK apoptosis signaling pathway (38). With respect to glutaminolysis, the rSCC-61 cells were less reliant on this pathway for proliferation compared with SCC-61, which had significantly decreased cell proliferation with glutamine deprivation. Glutamine is a nonessential versatile amino acid with multiple functions in nucleotide, protein, lipid and ATP biosynthesis (39). It should also be noted that cancer cells show systemic differences in their glutamine dependence and that not all cancer

cells require exogenous supply of glutamine (40). Resistance to glutamine metabolism has also been associated with *de novo* biosynthesis of glutamine or utilization of alternate anaplerotic pathways (40). Whether rSCC-61 bypasses glutamine metabolism or redirects glutamine biosynthesis along with its functional consequence to resistance to radiation remains to be explored. Radiation treatment significantly impaired cell proliferation when used alone. However, an additive or synergistic effect, when used in combination with inhibitors of cellular energy metabolism, was not evident from the studies reported here suggesting either: 1. masking of the radiation-induced cell death due to the much stronger effects of energy deprivation; or 2. dependence of radiation effects on energy metabolism. We favor the second scenario based on the known mechanisms of radiation-induced ROS and ROS amplification in time (41) and data showing an inhibition of the radiation-induced bystander effects and cell death in G6PD null cells (42).

Recent research has identified mitochondrial respiration as an important contributor to tumor cell survival and proliferation (12). Previous observations, such as reduced intracellular and extracellular lactate in rSCC-61 cells (24), have suggested potential deviation of rSCC-61 from the classical Warburg phenotype and channeling of pyruvate into the TCA cycle to support mitochondrial OXPHOS or into PPP to promote NADPH and nucleotide synthesis. To investigate this metabolic restructuring in rSCC-61, we measured the mitochondrial activity (OCR) in SCC-61 and rSCC-61 cells using the Seahorse XF analyzer. rSCC-61 cells had significantly lower basal OCR, indicating that these cells generate less ATP via mitochondrial respiration. Another significant observation was the lower spare capacity in rSCC-61 compared with SCC-61 ($P < 0.001$). It has been demonstrated that under stress mitochondria can draw on the spare capacity to meet the additional energy demands for detoxification and repair of stress-induced damage (43). Thus, intuitively we expected the spare capacity in rSCC-61 to be higher than SCC-61, a hypothesis that was proven incorrect by the analysis shown in Fig. 4. However, despite the lower spare capacity in rSCC-61, the rSCC-61 cells maintain a significant level of ATP production that could potentially be used to repair radiation-associated damage. Interestingly, the nonmitochondrial respiration was also decreased in rSCC-61 (though the statistical significance was lower compared to other OCR parameters) and was inhibited by orlistat treatment in both SCC-61 and rSCC-61 cells. A full investigation of the ROS sources and metabolism in SCC-61 and rSCC-61 cells is underway, but these results raise the possibility that other cellular oxygen-consuming reactions such as those catalyzed by cell membrane-associated NAD(P)H oxidases or oxidoreductases may contribute to both ROS content and energy metabolism by regenerating, for example, NAD^+ needed for glycolysis (44). Fatty acid metabolism may well contribute to these processes since there is an established regulatory relationship between plasma membrane lipid composition and activity of the enzymes embedded or associated with cellular plasma membrane (45). We plan to study these mechanisms as we further investigate this model of radiation resistance.

Fatty acids are also key contributors to energy metabolism, and key enzymes in the lipid synthesis pathway such as FASN have been shown to be upregulated in cancer cells (31). While a number of studies implicate the role of FASN in tumorigenesis and appreciate its diagnostic and prognostic value, studies focusing on the association of FASN

overexpression with response to therapy are limited. In head and neck cancer, overexpression of FASN has been previously reported and associated with lung metastasis of HNSCC and radiation resistance in nasopharyngeal cancer (46–49). Consistent with these observations, we found increased expression and activity of FASN in radiation-resistant rSCC-61 cells. Moreover, we demonstrate that inhibition of FASN by orlistat reduces rSCC-61 cell proliferation, and depletion of FASN with orlistat or siRNA renders the rSCC-61 cells sensitive to the cytotoxic effects of radiation. Depletion of FASN with orlistat significantly decreased ATP production in rSCC-61, thereby potentially reducing its ability to repair radiation-induced damage. We are particularly intrigued by a recent study showing the induction of epithelial-to-mesenchymal transition by decreasing the expression of FASN (50). These results match nicely with our previously reported analysis of the mesenchymal-to-epithelial change in phenotype in SCC-61/rSCC-61 system, which was associated with increased FASN expression in rSCC-61 (24). Together these studies point not only to the potential value of exploring FASN inhibitors for treatment of radiation-resistant HNSCC, but also to lipid metabolism as a major driver of radiation response and cellular epithelial or mesenchymal phenotype.

To summarize, we present an analysis of the nutrient and energy metabolism in a matched model of radiation resistance for HNSCC (Fig. 7). The radioresistant rSCC-61 cells were distinctly characterized by increased dependency on glucose and enhanced sensitivity to glycolysis and PPP inhibitors. The radiation-resistant phenotype was associated with a deviation from the Warburg effect and utilization of endogenous fatty acids for energy production. One of the significant findings of our study was the increased sensitivity to radiation upon inhibition of FASN, which opens new directions for research focused on development and optimization of inhibitors targeting lipid metabolism pathways that are enhanced in radiation-resistant HNSCC.

Acknowledgments

Research reported in this article was supported by the National Cancer Institute of the National Institutes of Health [R01 CA136810 (CMF)]. The authors acknowledge financial support from Wake Forest School of Medicine (development funds to CMF) and the Wake Forest University Structural and Computational Biophysics training program [T32GM095440 (predoctoral fellowship to JM)]. A National Science Foundation Major Research Instrumentation award supported the purchase of the LSCM used to generate GLUT1 images included in this article (MRI-0722926) within the WFU Microscopic Imaging Core Facility. The authors would also like to thank Dr. Glen Marrs (WFU) for advice on the imaging studies, Dr. Tiefu Liu in Dr. Charles McCall's laboratory (WFSM) for technical support with the palmitate uptake assay, Drs. Achche Patel and Weiling Zhao for technical assistance with some of the studies included here and Dr. Steven Kridel (WFSM) for advice on the FASN/orlistat studies.

References

1. Bernstein JM, Bernstein CR, West CM, Homer JJ. Molecular and cellular processes underlying the hallmarks of head and neck cancer. Eur Arch Otorhinolaryngol. 2012; 270:2585–93. [PubMed: 23263268]
2. Bentzen SM, Atasoy BM, Daley FM, Dische S, Richman PI, Saunders MI, et al. Epidermal growth factor receptor expression in pretreatment biopsies from head and neck squamous cell carcinoma as a predictive factor for a benefit from accelerated radiation therapy in a randomized controlled trial. J Clin Oncol. 2005; 26:5560–7. [PubMed: 16110017]
3. Bonner JA, Harari PM, Giralt J, Azarnia N, Shin DM, Cohen RB, et al. Radiotherapy plus cetuximab for squamous-cell carcinoma of the head and neck. N Engl J Med. 2006; 354:567–78. [PubMed: 16467544]

4. Harari PM, Huang S. Radiation combined with EGFR signal inhibitors: head and neck cancer focus. Semin Radiat Oncol. 2006; 16:38–44. [PubMed: 16378905]
5. Hanahan D, Weinberg RA. Hallmarks of cancer: the next generation. Cell. 2011; 144:646–74. [PubMed: 21376230]
6. Hanahan D, Weinberg RA. The hallmarks of cancer. Cell. 2000; 100:57–70. [PubMed: 10647931]
7. Barger JF, Plas DR. Balancing biosynthesis and bioenergetics: metabolic programs in oncogenesis. Endocr Relat Cancer. 2010; 17:R287–304. [PubMed: 20699334]
8. Wise DR, DeBerardinis RJ, Mancuso A, Sayed N, Zhang XY, Pfeiffer HK, et al. Myc regulates a transcriptional program that stimulates mitochondrial glutaminolysis and leads to glutamine addiction. Proc Natl Acad Sci U S A. 2008; 105:18782–7. [PubMed: 19033189]
9. Warburg O. On the origin of cancer cells. Science. 1956; 123:309–14. [PubMed: 13298683]
10. Vander Heiden MG, Cantley LC, Thompson CB. Understanding the Warburg effect: the metabolic requirements of cell proliferation. Science. 2009; 324:1029–33. [PubMed: 19460998]
11. Koppenol WH, Bounds PL, Dang CV. Otto Warburg's contributions to current concepts of cancer metabolism. Nat Rev Cancer. 2011; 11:325–37. [PubMed: 21508971]
12. Ward PS, Thompson CB. Metabolic reprogramming: a cancer hallmark even Warburg did not anticipate. Cancer Cell. 2012; 21:297–308. [PubMed: 22439925]
13. Cairns RA, Harris IS, Mak TW. Regulation of cancer cell metabolism. Nat Rev Cancer. 2011; 11:85–95. [PubMed: 21258394]
14. Weinberg F, Hamanaka R, Wheaton WW, Weinberg S, Joseph J, Lopez M, et al. Mitochondrial metabolism and ROS generation are essential for Kras-mediated tumorigenicity. Proc Natl Acad Sci U S A. 2010; 107:8788–93. [PubMed: 20421486]
15. Pike LS, Smift AL, Croteau NJ, Ferrick DA, Wu M. Inhibition of fatty acid oxidation by etomoxir impairs NADPH production and increases reactive oxygen species resulting in ATP depletion and cell death in human glioblastoma cells. Biochim Biophys Acta. 2011; 1807:726–34. [PubMed: 21692241]
16. Diers AR, Broniowska KA, Chang CF, Hogg N. Pyruvate fuels mitochondrial respiration and proliferation of breast cancer cells: effect of monocarboxylate transporter inhibition. Biochem J. 2012; 444:561–71. [PubMed: 22458763]
17. Sandulache VC, Ow TJ, Pickering CR, Frederick MJ, Zhou G, Fokt I, et al. Glucose, not glutamine, is the dominant energy source required for proliferation and survival of head and neck squamous carcinoma cells. Cancer. 2011; 117:2926–38. [PubMed: 21692052]
18. Simons AL, Parsons AD, Foster KA, Orcutt KP, Fath MA, Spitz DR. Inhibition of glutathione and thioredoxin metabolism enhances sensitivity to perifosine in head and neck cancer cells. J Oncol. 2009; 2009:519563. [PubMed: 19746172]
19. Tripathi P, Kamarajan P, Somashekar BS, MacKinnon N, Chinnaiyan AM, Kapila YL, et al. Delineating metabolic signatures of head and neck squamous cell carcinoma: phospho-lipase A2, a potential therapeutic target. Int J Biochem Cell Biol. 2012; 44:1852–61. [PubMed: 22743333]
20. Yang C, Sudderth J, Dang T, Bachoo RM, McDonald JG, DeBerardinis RJ. Glioblastoma cells require glutamate dehydro-genase to survive impairments of glucose metabolism or Akt signaling. Cancer Res. 2009; 69:7986–93. [PubMed: 19826036]
21. Maschek G, Savaraj N, Priebe W, Braunschweiger P, Hamilton K, Tidmarsh GF, et al. 2-deoxy-D-glucose increases the efficacy of adriamycin and paclitaxel in human osteosarcoma and non-small cell lung cancers in vivo. Cancer Res. 2004; 64:31–4. [PubMed: 14729604]
22. Mohanti BK, Rath GK, Anantha N, Kannan V, Das BS, Chandramouli BA, et al. Improving cancer radiotherapy with 2-deoxy-D-glucose: phase I/II clinical trials on human cerebral gliomas. Int J Radiat Oncol Biol Phys. 1996; 35:103–11. [PubMed: 8641905]
23. Dwarakanath BS, Singh D, Banerji AK, Sarin R, Venkataramana NK, Jalali R, et al. Clinical studies for improving radiotherapy with 2-deoxy-D-glucose: present status and future prospects. J Cancer Res Ther. 2009; 5(Suppl 1):S21–6. [PubMed: 20009289]
24. Bansal N, Mims J, Kuremsky JG, Olex AL, Zhao W, Yin L, et al. Broad phenotypic changes associated with gain of radiation resistance in head and neck squamous cell cancer. Antioxid Redox Signal. 2014; 21:221–36. [PubMed: 24597745]

25. Vichai V, Kirtikara K. Sulforhodamine B colorimetric assay for cytotoxicity screening. Nat Protoc. 2006; 1:1112–6. [PubMed: 17406391]
26. Bensaad K, Tsuruta A, Selak MA, Vidal MN, Nakano K, Bartrons R, et al. TIGAR, a p53-inducible regulator of glycolysis and apoptosis. Cell. 2006; 126:107–20. [PubMed: 16839880]
27. Robey RB, Hay N. Mitochondrial hexokinases, novel mediators of the antiapoptotic effects of growth factors and Akt. Oncogene. 2006; 25:4683–96. [PubMed: 16892082]
28. DeBerardinis RJ, Lum JJ, Hatzivassiliou G, Thompson CB. The biology of cancer: metabolic reprogramming fuels cell growth and proliferation. Cell Metab. 2008; 7:11–20. [PubMed: 18177721]
29. Yuneva M, Zamboni N, Oefner P, Sachidanandam R, Lazebnik Y. Deficiency in glutamine but not glucose induces MYC-dependent apoptosis in human cells. J Cell Biol. 2007; 178:93–105. [PubMed: 17606868]
30. Ralser M, Wamelink MM, Struys EA, Joppich C, Krobitsch S, Jakobs C, et al. A catabolic block does not sufficiently explain how 2-deoxy-D-glucose inhibits cell growth. Proc Natl Acad Sci U S A. 2008; 105:17807–11. [PubMed: 19004802]
31. Menendez JA, Lupu R. Fatty acid synthase and the lipogenic phenotype in cancer pathogenesis. Nat Rev Cancer. 2007; 7:763–77. [PubMed: 17882277]
32. Corvo R. Evidence-based radiation oncology in head and neck squamous cell carcinoma. Radiother Oncol. 2007; 85:156–70. [PubMed: 17482300]
33. Nutting CM, Bhide SA, Harrington KJ. Treatment of head and neck cancer. N Engl J Med. 2008; 358:1076–7. author reply 77–8. [PubMed: 18326077]
34. Forastiere AA, Trotti A, Pfister DG, Grandis JR. Head and neck cancer: recent advances and new standards of care. J Clin Oncol. 2006; 24:2603–5. [PubMed: 16763271]
35. Sandulache VC, Myers JN. Altered metabolism in head and neck squamous cell carcinoma: an opportunity for identification of novel biomarkers and drug targets. Head Neck. 2012; 34:282–90. [PubMed: 21322078]
36. Somashekar BS, Kamarajan P, Danciu T, Kapila YL, Chinnaiyan AM, Rajendiran TM, et al. Magic angle spinning NMR-based metabolic profiling of head and neck squamous cell carcinoma tissues. J Proteome Res. 2011; 10:5232–41. [PubMed: 21961579]
37. Kunkel M, Reichert TE, Benz P, Lehr HA, Jeong JH, Wieand S, et al. Overexpression of Glut-1 and increased glucose metabolism in tumors are associated with a poor prognosis in patients with oral squamous cell carcinoma. Cancer. 2003; 97:1015–24. [PubMed: 12569601]
38. Sharma PK, Varshney R. 2-Deoxy-D-glucose and 6-aminonicotin-amide-mediated Nrf2 down regulation leads to radiosensitization of malignant cells via abrogation of GSH-mediated defense. Free Radic Res. 2012; 46:1446–57. [PubMed: 22946929]
39. Daye D, Wellen KE. Metabolic reprogramming in cancer: unraveling the role of glutamine in tumorigenesis. Semin Cell Dev Biol. 2012; 23:362–9. [PubMed: 22349059]
40. Hensley CTWA, DeBerardinis RJ. Glutamine and cancer: cell biology, physiology, and clinical opportunities. J Clin Invest. 2013; 123:3678–84. [PubMed: 23999442]
41. Reisz JA, Bansal N, Qian J, Zhao W, Furdui CM. Effects of ionizing radiation on biological molecules-mechanisms of damage and emerging methods of detection. Antioxid Redox Signal. 2014; 21:260–92. [PubMed: 24382094]
42. Mothersill C, Stamato TD, Perez ML, Cummins R, Mooney R, Seymour CB. Involvement of energy metabolism in the production of ‘bystander effects’ by radiation. Br J Cancer. 2000; 82:1740–6. [PubMed: 10817512]
43. Hill BG, Dranka BP, Zou L, Chatham JC, Darley-Usmar VM. Importance of the bioenergetic reserve capacity in response to cardiomyocyte stress induced by 4-hydroxynonenal. Biochem J. 2009; 424:99–107. [PubMed: 19740075]
44. Herst PM, Berridge MV. Plasma membrane electron transport: a new target for cancer drug development. Curr Mol Med. 2006; 6:895–904. [PubMed: 17168740]
45. Jin S, Zhou F, Katirai F, Li PL. Lipid raft redox signaling: molecular mechanisms in health and disease. Antioxid Redox Signal. 2011; 15:1043–83. [PubMed: 21294649]

46. Benevenuto de Andrade BA, Pina AR, Leon JE, Paes de Almeida O, Altemani A. Primary nasal mucosal melanoma in Brazil: clinicopathologic and immunohistochemical study of 12 patients. Ann Diagn Pathol. 2012; 16:344–9. [PubMed: 22425483]

47. De Vincentiis M, Di Cello P, Censi F, Leopizzi M, Natalizi S, Sardella B, et al. Immunohistochemical expression of fatty acid synthase, Ki-67 and p53 in squamous cell carcinomas of the larynx. Int J Biol Markers. 2008; 23:176–81. [PubMed: 18949744]

48. Kao YC, Lee SW, Lin LC, Chen LT, Hsing CH, Hsu HP, et al. Fatty acid synthase overexpression confers an independent prognosticator and associates with radiation resistance in naso-pharyngeal carcinoma. Tumour Biol. 2012; 34:759–68. [PubMed: 23208675]

49. Silva SD, Cunha IW, Younes RN, Soares FA, Kowalski LP, Graner E. ErbB receptors and fatty acid synthase expression in aggressive head and neck squamous cell carcinomas. Oral Dis. 2010; 16:774–80. [PubMed: 20604875]

50. Jiang L, Xiao L, Sugiura H, Huang X, Ali A, Kuro OM, et al. Metabolic reprogramming during TGFbeta1-induced epithelial-to-mesenchymal transition. Oncogene. 2014 (Epub ahead of print). 10.1038/onc.2014.321

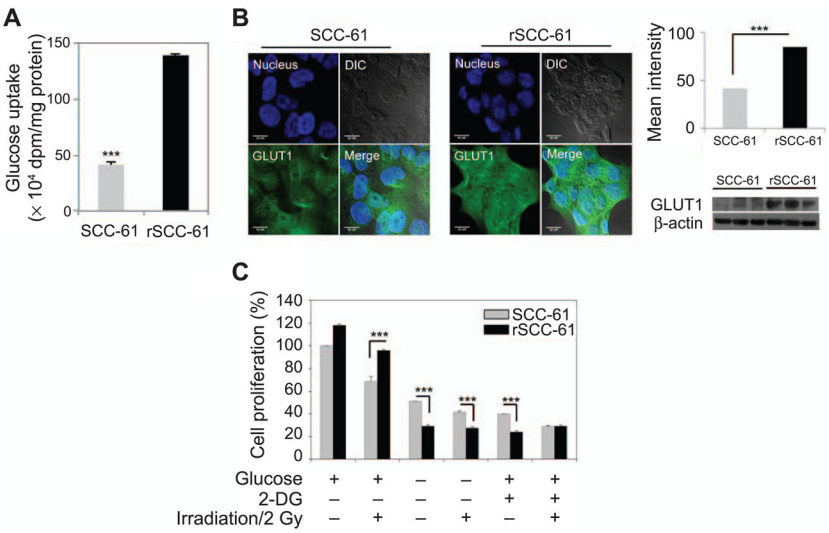

FIG. 1.

Glucose uptake and dependence of cell growth on glucose metabolism in SCC-61 and rSCC-61 cells. Panel A: Assay showing increased glucose uptake in rSCC-61 compared to SCC-61 cells (***$P < 0.001$). Panel B: Imaging analysis of GLUT1 (green) in SCC-61 and rSCC-61 cells, quantification of imaging data and validation by Western blot. Blue: Hoechst nucleus staining. The differential contrast images (DIC) and merge panels are also shown. Increased GLUT1 staining and expression by Western blot was observed in rSCC-61 consistent with the glucose uptake data. The scale bars represent a distance of 20 μm (***$P < 0.001$). Panel C: Glucose deprivation (–) or 2-DG treatment (+) effects on cell proliferation with or without irradiation (–/+). Cell proliferation is expressed as percentage relative to the untreated SCC-61 cells in the absence of radiation exposure. Compared to SCC-61, the rSCC-61 cells have increased requirement of glucose for survival and enhanced sensitivity to the metabolic inhibitor 2-DG regardless of radiation treatment. The statistical analysis is based on three biological replicates (***$P < 0.001$).

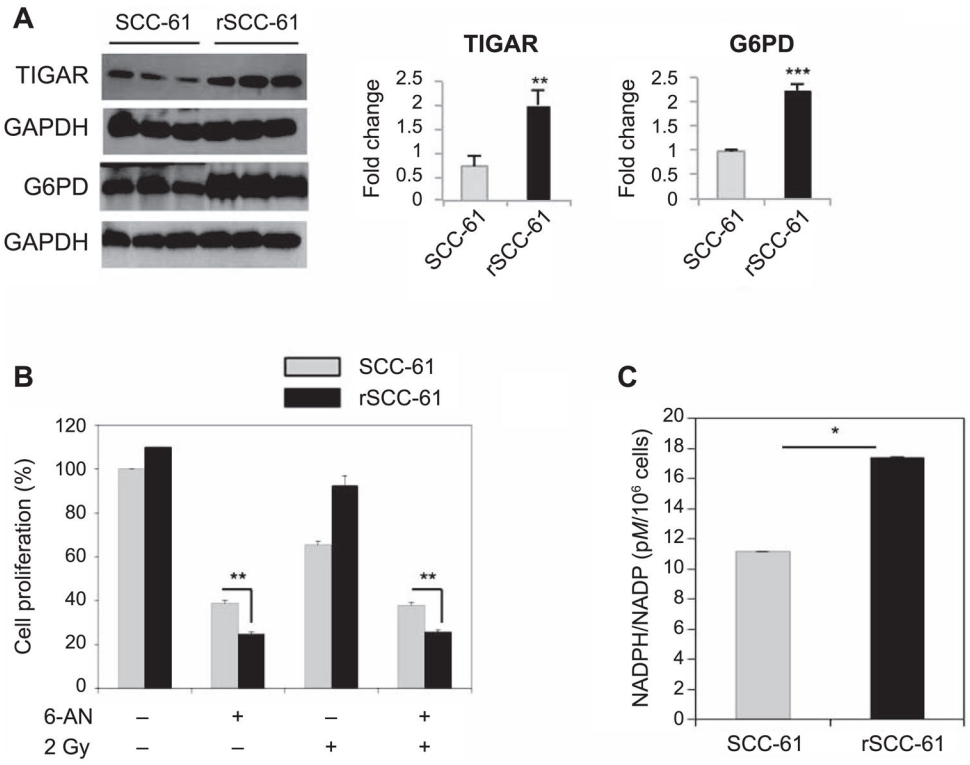

FIG. 2.

Contribution of PPP to cellular proliferation in SCC-61 and rSCC-61 cells. Panel A: Western blot analysis showing increased expression of TIGAR (***P* = 0.004) and glucose 6-phosphate dehydrogenase (G6PD) (****P* < 0.001) in rSCC-61 compared with SCC-61. Panel B: Cell proliferation with or without 6-AN treatment, a PPP inhibitor targeting 6-phosphogluconate dehydrogenase (***P* = 0.008) and 2 Gy irradiation (***P* = 0.005). Cell proliferation was measured using the sulforhodamine B (SRB) assay and expressed as percentage relative to the untreated control. Three biological replicates were used in this analysis. The results show increased dependence on PPP in rSCC-61 cells compared with SCC-61 cells before and after irradiation. Panel C: NADPH/$NADP^+$ quantification showing increased NADPH in rSCC-61 cells compared to SCC-61 cells (***P*= 0.04).

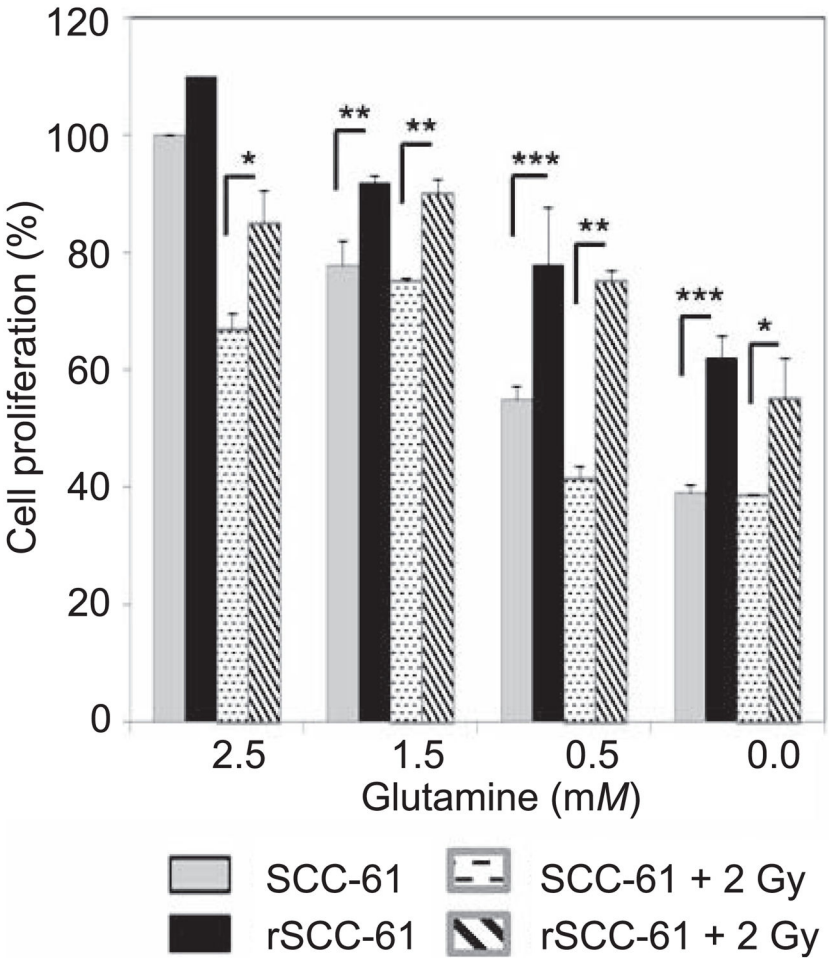

FIG. 3.

Glutamine utilization in SCC-61 and rSCC-61 cells. Cell proliferation using media supplemented with decreasing concentrations of glutamine and either without or with irradiation (e.g., ***$P < 0.001$ and *$P = 0.04$ for 0.0 m*M* glutamine, without irradiation and with 2 Gy irradiation, respectively). SRB assay for cell proliferation was performed using three biological replicates for each treatment condition. The results show an overall increased reliance on glutamine metabolism in SCC-61 compared with rSCC-61 cells.

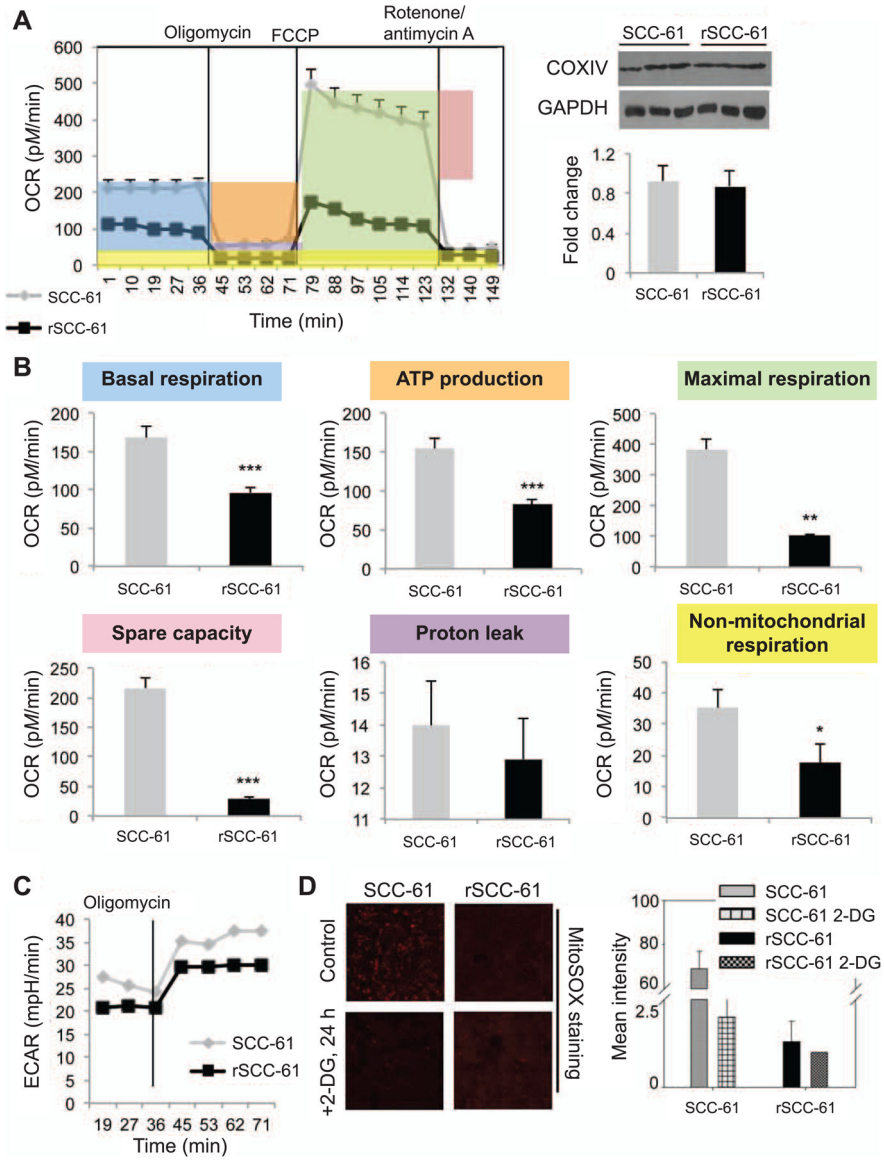

FIG. 4.

rSCC-61 has decreased OXPHOSP capabilities. Panel A: Oxygen consumption rate (OCR) for SCC-61 and rSCC-61 cells using Seahorse XFA 24-3. As shown in the OCR profile plot, the first five measurements represent OCR of untreated cells followed by sequential addition of three mitochondrial inhibitors (after measurements 5, 9 and 15, respectively). Right panel shows the CoxIV Western blot demonstrating equal mitochondrial content in the two cells lines. Panel B: Statistical analysis and representative plots extracted from the study in panel A. The *P* values are as follows: basal respiration ***$P < 0.001$; ATP production ***$P < 0.001$; maximal respiration **$P = 0.006$; spare capacity ***$P < 0.001$; and nonmitochondrial respiration *$P = 0.03$. Panel C: Extracellular acidification rate (ECAR) data showing increased ECAR in SCC-61 (n = 5). Panel D: Imaging analysis of mitochondrial ROS using MitoSOX staining for superoxide in SCC-61 and rSCC-61 cells untreated and treated with 20 m*M* 2-DG for 24 h.

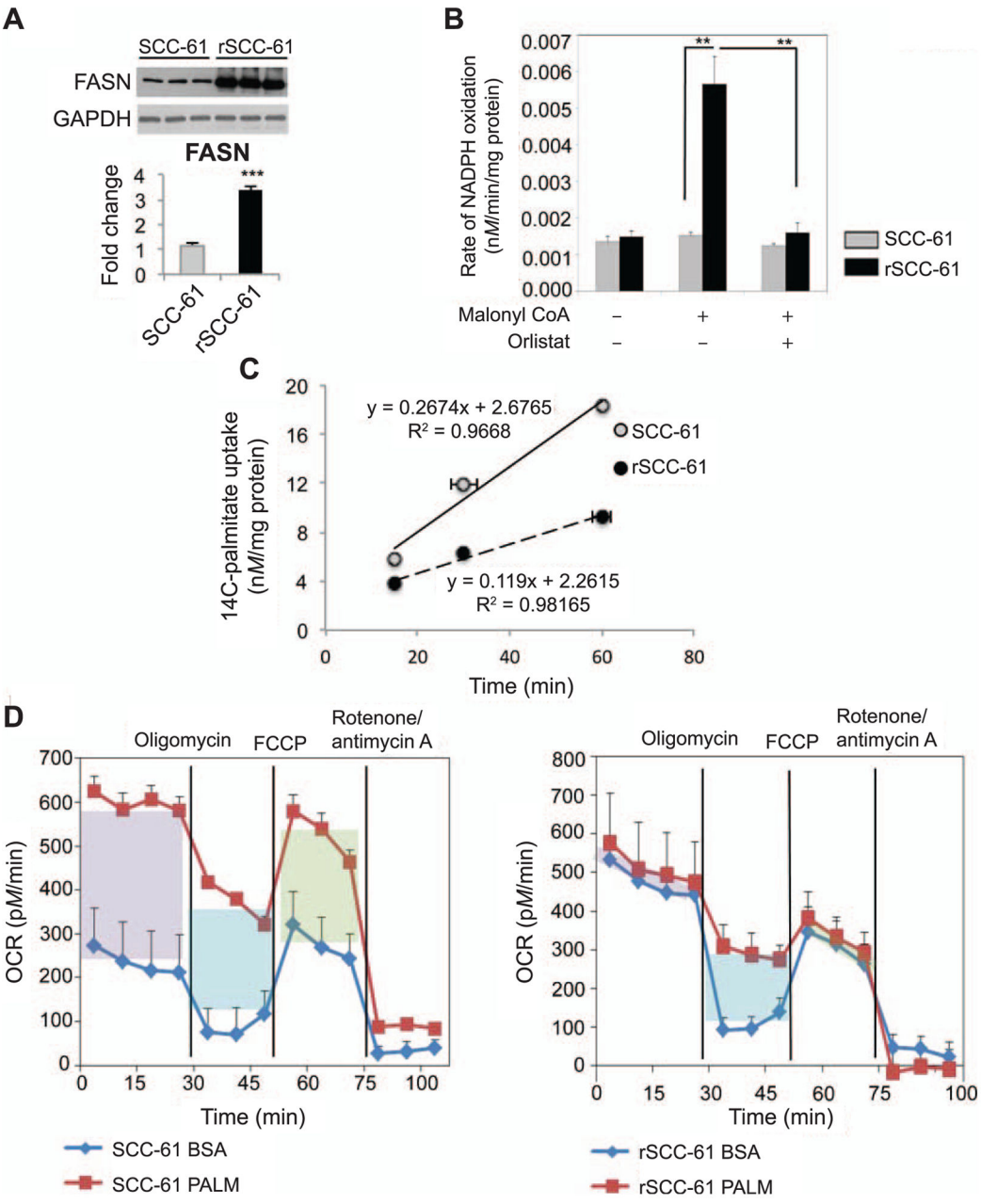

FIG. 5.

Fatty acid synthase is overexpressed and correlated to radioresistance in rSCC-61. Panel A: Western blot analysis of FASN and quantification ($P < 0.001$) showing increased expression in rSCC-61 cells. GAPDH staining was performed to show equal protein loading. Panel B: Fatty acid synthase activity assay. FASN-dependent oxidation of NADPH with or without orlistat treatment was measured as described in the Materials and Methods section. rSCC-61 have significantly higher ($P < 0.01$) FASN activity that is reduced upon the addition of the FASN inhibitor orlistat. Panel C: ^{14}C-Palmitate uptake. SCC-61 and rSCC-61 were cultured and incubating with ^{14}C-palmitate for 15, 30 and 60 min. Exogenous palmitate uptake in rSCC-61 cells was twofold lower than in SCC-61. Panel D: Fatty acid oxidation assay.

SCC-61 cells demonstrate a significant reliance on utilization of exogenous palmitate to respond to energy demand compared to rSCC-61. Purple box: basal respiration; blue box: uncoupling of mitochondria; green box: maximal respiration.

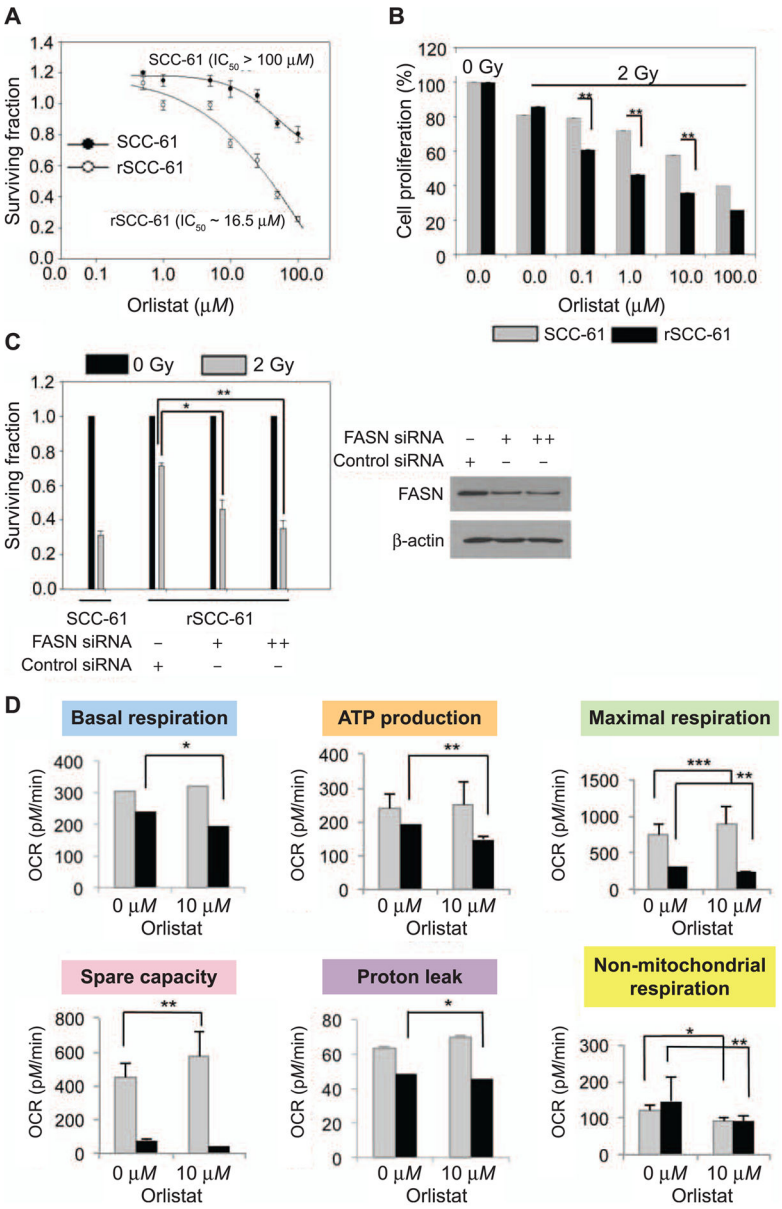

FIG. 6.

Panel A: Clonogenic assay to determine the response to orlistat treatment. The survival plots for the SCC-61 and rSCC-61 cells are shown in response to increasing doses of orlistat. The calculated IC_{50} for orlistat in each cell line is indicated and show enhanced sensitivity to orlistat treatment in rSCC-61. Panel B: Cell proliferation in the presence of increasing concentrations of orlistat and 2 Gy irradiation was determined using the SRB assay (**P = 0.009, **P = 0.005, **P = 0.007 for 0.1, 1 and 10.0 μM orlistat, respectively). Three biological replicates were used for each study. The results show increased sensitivity to radiation after treatment with orlistat in rSCC-61 compared with SCC-61 cells. Panel C: Clonogenic assay to determine the radiosensitizing effect of FASN depletion. rSCC-61 cells transfected with control or FASN siRNA were set up for clonogenic assays and their survival was calculated with 2 Gy irradiation or without irradiation. siRNA-mediated

depletion of FASN protein significantly radiosensitized rSCC-61 cells (**P = 0.001–0.01). SCC-61 cells were also set up alongside for the assay for a comparative overview of radiosensitivity. Panel D: OCR for SCC-61 and rSCC-61 cells using Seahorse XFA 24-3 after treatment with 10 μM orlistat. Inhibition of FASN by orlistat significantly decreased mitochondrial OCR in rSCC-61 cells and impacted the nonmitochondrial OCR in both SCC-61 and rSCC-61 cells (*P = 0.01–0.05, **P = 0.001–0.01 and ***P < 0.001).

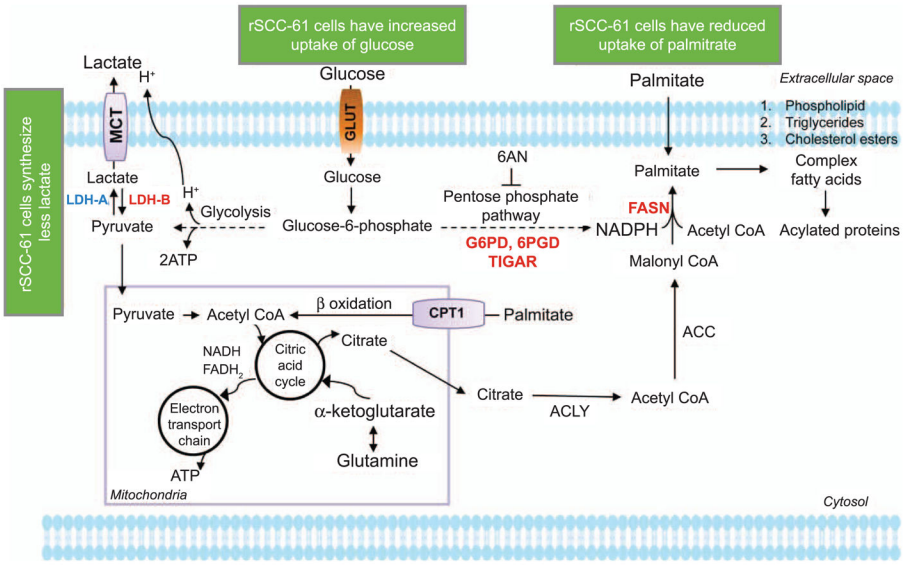

FIG. 7.

Summary overview of the differential carbohydrate and lipid metabolism in SCC-61 and rSCC-61 cells. 6-AN = 6-aminonicotinamide; G6PD = glucose 6-phosphate dehydrogenase; 6PGD = 6-phosphogluconate dehydrogenase; ACC = acetyl-CoA carboxylase; ACLY = ATP:citrate lyase; CPT1 = carnitine palmitoyl-transferase I; FASN = fatty acid synthase; GLUT = glucose transporter; LDHA/B = lactate dehydrogenase A/B; MCT = monocarboxylate transporter; TIGAR = TP53-inducible glycolysis and apoptosis regulator.